Inorg. Chem. **2008**, *47*, 6889−6899

Inorganic Chemistry
Article

Europium(III) Reduction and Speciation within a Wells−Dawson Heteropolytungstate

Jing Jing,[†] Benjamin P. Burton-Pye,[†] Lynn C. Francesconi,*[,†] and Mark R. Antonio*[,‡]

Department of Chemistry, Hunter College and the Graduate School of the City University of New York, New York, New York 10021, Chemical Sciences & Engineering Division, Argonne National Laboratory, Argonne, Illinois 60439

Received March 13, 2008

The redox speciation of Eu(III) in the 1:1 stoichiometric complex with the α-1 isomer of the Wells−Dawson anion, $[\alpha\text{-}1\text{-}P_2W_{17}O_{61}]^{10-}$, was studied by electrochemical techniques (cyclic voltammetry and bulk electrolysis), in situ XAFS (X-ray absorption fine structure) spectroelectrochemistry, NMR spectroscopy (^{31}P), and optical luminescence. Solutions of $K_7[(H_2O)_4Eu(\alpha\text{-}1\text{-}P_2W_{17}O_{61})]$ in a 0.2 M Li_2SO_4 aqueous electrolyte (pH 3.0) show a pronounced concentration dependence to the voltammetric response. The fully oxidized anion and its reduced forms were probed by Eu L_3-edge XANES (X-ray absorption near edge structure) measurements in simultaneous combination with controlled potential electrolysis, demonstrating that Eu(III) in the original complex is reduced to Eu(II) in conjunction with the reduction of polyoxometalate (POM) ligand. After exhaustive reduction, the heteropoly blue species with Eu(II) is unstable with respect to cluster isomerization, fragmentation, and recombination to form three other Eu-POMs as well as the parent Wells−Dawson anion, $\alpha\text{-}[P_2W_{18}O_{62}]^{6-}$. EXAFS data obtained for the reduced, metastable Eu(II)-POM before the onset of Eu(II) autoxidation provides an average Eu−O bond length of 2.55(4) Å, which is 0.17 Å longer than that for the oxidized anion, and consistent with the 0.184 Å difference between the Eu(II) and Eu(III) ionic radii. The reduction of Eu(III) is unusual among POM complexes with Lindqvist and α-2 isomers of Wells−Dawson anions, that is, $[Eu(W_5O_{18})_2]^{9-}$ and $[Eu(\alpha\text{-}2\text{-}As_2W_{17}O_{61})_2]^{17-}$, but not to the Preyssler complex anion, $[EuP_5W_{30}O_{110}]^{12-}$, and fundamental studies of materials based on coupling Eu and POM redox properties are still needed to address new avenues of research in europium hydrometallurgy, separations, and catalysis sciences.

Introduction

Lanthanide (Ln) interactions with polyoxometalate (POM) anions are of contemporary interest, both fundamentally and practically, as a consequence of the formation of high-nuclearity clusters with complex architectures assembled from oxo linkage connectivities of f and d elements, −Ln(III)−O−M(VI)− for M = Mo and W.[1–20] The resulting Ln-POM clusters offer unique functionalities and properties as luminescent materials, particularly the Eu-POMs,[18,19] and as selective and recoverable Lewis acid catalysts.[20,21] Moreover, prospective and realized applications in areas of

* To whom correspondence should be addressed. E-mail: lfrances@hunter.cuny.edu (L.C.F.); mantonio@anl.gov (M.R.A.).
[†] Hunter College and the Graduate School of the City University of New York.
[‡] Argonne National Laboratory.

(1) Cronin, L.; Beugholt, C.; Krickemeyer, E.; Schmidtmann, M.; Bogge, H.; Kogerler, P.; Luong, T. K. K.; Muller, A. *Angew. Chem., Int. Ed.* **2002**, *41*, 2805–2808.
(2) Fukaya, K.; Yamase, T. *Angew. Chem., Int. Ed.* **2003**, *42*, 654–658.
(3) Howell, R. C.; Perez, F. G.; Jain, S.; Horrocks, W. D.; Rheingold, A. L.; Francesconi, L. C. *Angew. Chem., Int. Ed.* **2001**, *40*, 4031–4034.
(4) Muller, A.; Beugholt, C.; Bogge, H.; Schmidtmann, M. *Inorg. Chem.* **2000**, *39*, 3112–3113.
(5) Muller, A.; Peters, F.; Pope, M. T.; Gatteschi, D. *Chem. Rev.* **1998**, *98*, 239–272.
(6) Ostuni, A.; Pope, M. T. *Comptes Rendus Acad. Sci. Ser. II C* **2000**, *3*, 199–204.
(7) Wassermann, K.; Dickman, M. H.; Pope, M. T. *Angew. Chem., Int. Ed.* **1997**, *36*, 1445–1448.
(8) Zimmermann, M.; Belai, N.; Butcher, R. J.; Pope, M. T.; Chubarova, E. V.; Dickman, M. H.; Kortz, U. *Inorg. Chem.* **2007**, *46*, 1737–1740.
(9) Bassil, B. S.; Dickman, M. H.; Von Kammer, B.; Kortz, U. *Inorg. Chem.* **2007**, *46*, 2452–2458.
(10) Belai, N.; Sadakane, M.; Pope, M. T. *J. Am. Chem. Soc.* **2001**, *123*, 2087–2088.
(11) Copping, R.; Gaunt, A. J.; May, I.; Sarsfield, M. J.; Collison, D.; Helliwell, M.; Denniss, I. S.; Apperley, D. C. *Dalton Trans.* **2005**, 1256–1262.
(12) Lu, Y. W.; Keita, B.; Nadjo, L. *Polyhedron* **2004**, *23*, 1579–1586.
(13) Mialane, P.; Lisnard, L.; Mallard, A.; Marrot, J.; Antic-Fidancev, E.; Aschehoug, P.; Vivien, D.; Secheresse, F. *Inorg. Chem.* **2003**, *42*, 2102–2108.

10.1021/ic800465e CCC: $40.75
Published on Web 07/11/2008

separations science, photophysics, and electroanalytical chemistry are founded upon the renown reduction−oxidation (redox) properties of POMs.[22,23] As such, the fusion of redox-active Ln ions, specifically the reducible Eu(III) ion and the oxidizable Ce(III) ion, with POMs provides molecular systems with hybrid electrochemical properties, such as seen in other hybrid systems that combine, for example, metallocenes, fullerenes,[24,25] and multinuclear exohedral metallofullerenes.[26] For Ln-POMs, the combination of the key electrofunctional properties of both the metal and the ligand in one molecule produces two-center, multielectron redox systems in which basic information about the interactions between the atomic-like Ln f orbitals and the band-like M d orbitals of POM ligands is largely unknown.

Although there are numerous reports about Eu-POMs,[1–3,9,17,19,27–33] the reduction of Eu(III) in these cluster anions is an unusual phenomenon and has only been observed for the Preyssler anion, $[EuP_5W_{30}O_{110}]^{12-}$.[34] This may be due to experimental difficulties of probing the Eu ion valence in opaque, heteropoly blue solutions of Eu-POMs, or, alternatively, that the energetics of the Eu 4f orbital interactions with LUMO states of essentially d orbital character are unfavorable. The first hurdle has been cleared by the application of in situ X-ray absorption near edge structure (XANES) spectroelectrochemistry to Ln- and actinide-POM science.[32,33,35] The second vis-à-vis the interaction of the localized Eu f states and the W−O d states may be due to stereochemical effects that either favor or hinder metal−ligand orbital mixing. For example, the connectivity of Eu(III) with the ligand LUMO is pivotal to reductive electrochemistry and, for the case of $[EuP_5W_{30}O_{110}]^{12-}$, experimental[36] and theoretical[37] results indicate that the spatial association of Eu(III) with the W ions that comprise the LUMO states is a principal factor in f−d electron coupling and non-Nernstian electrochemical behavior.[34]

In similar regard, geometric factors concerning the complexation of Eu(III) by isomers of the monovacant Wells−Dawson anion, $[P_2W_{17}O_{61}]^{10-}$, may influence Eu reduction. In complexes with both the α-1 and α-2 isomers, Eu is bonded to the P−W−O ligands by four O atoms, which serve as μ-oxo bridges between Eu(III) and 4 W(VI) sites of which, for the α-1 isomer, 3 occupy belt positions and 1 occupies a cap position, and, for the α-2 isomer, 2 are in belt and 2 are in cap positions (Figure 1). Each of the 17 W(VI) ion positions in the P−W−O framework structure of the α-1 isomer are magnetically inequivalent.[30,38–41] Of particular significance here is that upon reduction of the fully oxidized anions, electrons are injected into the LUMO states that are centered on the W ions in the belt regions of the anions.[42,43] As such, heterometal cations, that is, Ln and transition metals, bound in the vacancies of the α-1 POM have one more direct connection with the W-centered LUMO states than do the heterometal complexes of the α-2 POM. A physical manifestation of these oxo linkage connectivities relates to reduction processes, wherein electroactive transition-metal cations at the α-1 site are more readily reduced than when substituted at the α-2 position.[44–49] The orientation of a basic oxygen atom, pointing at the α-1 site, from the adjoining $[PO_4]^{3-}$ tetrahedron around which the W−O framework is assembled also favors stronger coupling of heterometal ions

(14) Ozeki, T.; Yamase, T. *Acta Crystallogr., Sect. B* **1994**, *50*, 128–134.
(15) Sadakane, M.; Dickman, M. H.; Pope, M. T. *Angew. Chem., Int. Ed.* **2000**, *39*, 2914–2916.
(16) Shiozaki, R.; Inagaki, A.; Nishino, A.; Nishio, E.; Maekawa, M.; Kominami, H.; Kera, Y. *J. Alloys Compd.* **1996**, *234*, 193–198.
(17) Sousa, F. L.; Ferreira, A.; Ferreira, R. A. S.; Cavaleiro, A. M. V.; Carlos, L. D.; Nogueira, H. I. S.; Rocha, J.; Trindade, T. *J. Nanosci. Nanotechnol.* **2004**, *4*, 214–220.
(18) Yamase, T. *Chem. Rev.* **1998**, *98*, 307–326.
(19) Yamase, T.; Kobayashi, T.; Sugeta, M.; Naruke, H. *J. Phys. Chem. A* **1997**, *101*, 5046–5053.
(20) Boglio, C.; Lemiere, G.; Hasenknopf, B.; Thorimbert, S.; Lacote, E.; Malacria, M. *Angew. Chem., Int. Ed.* **2006**, *45*, 3324–3327.
(21) Boglio, C.; Lenoble, G.; Duhayon, C.; Hasenknopf, B.; Thouvenot, R.; Zhang, C.; Howell, R. C.; Burton-Pye, B. P.; Francesconi, L. C.; Lacote, E.; Thorimbert, S.; Malacria, M.; Afonso, C.; Tabet, J.-C. *Inorg. Chem.* **2006**, *45*, 1389–1398.
(22) Keita, B.; Nadjo, L. In *Encyclopedia of Electrochemistry*; Scholz, F., Pickett, C. J., Eds.; Wiley-VCH: Weiheim, 2006; Vol. 7b; pp 607−700.
(23) Weinstock, I. A. *Chem. Rev.* **1998**, *98*, 113–170.
(24) Guldi, D. M.; Rahman, G. M. A.; Marczak, R.; Matsuo, Y.; Yamanaka, M.; Nakamura, E. *J. Am. Chem. Soc.* **2006**, *128*, 9420–9427.
(25) Matsuo, Y.; Muramatsu, A.; Kamikawa, Y.; Kato, T.; Nakamura, E. *J. Am. Chem. Soc.* **2006**, *128*, 9586–9587.
(26) Park, B. K.; Lee, G.; Kim, K. H.; Kang, H.; Lee, C. Y.; Miah, M. A.; Jung, J.; Han, Y. K.; Park, J. T. *J. Am. Chem. Soc.* **2006**, *128*, 11160–11172.
(27) Zhang, C.; Howell, R. C.; Scotland, K. B.; Perez, F. G.; Todaro, L.; Francesconi, L. C. *Inorg. Chem.* **2004**, *43*, 7691–7701.
(28) Zhang, C.; Howell, R. C.; McGregor, D.; Bensaid, L.; Rahyab, S.; Nayshtut, M.; Lekperic, S.; Francesconi, L. C. *C. R. Chim.* **2005**, *8*, 1035–1044.
(29) Fukaya, K.; Yamase, T. *J. Alloys Compd.* **2006**, *408*, 915–920.
(30) Bartis, J.; Dankova, M.; Lessmann, J. J.; Luo, Q.-H.; De Horrocks, W., Jr.; Francesconi, L. C. *Inorg. Chem.* **1999**, *38*, 1042–1053.
(31) Ozeki, T.; Yamase, T.; Naruke, H.; Sasaki, Y. *Inorg. Chem.* **1994**, *33*, 409–410.
(32) Antonio, M. R.; Soderholm, L. *J. Cluster Sci.* **1996**, *7*, 585–591.
(33) Antonio, M. R.; Soderholm, L.; Jennings, G.; Francesconi, L. C.; Dankova, M.; Bartis, J. *J. Alloys Compd.* **1998**, 275–277, 827−830.
(34) Soderholm, L.; Antonio, M. R.; Skanthakumar, S.; Williams, C. W. *J. Am. Chem. Soc.* **2002**, *124*, 7290–7291.
(35) Antonio, M. R.; Soderholm, L.; Williams, C. W.; Ullah, N.; Francesconi, L. C. *Dalton Trans.* **1999**, 3825–3830.
(36) Chiang, M. H.; Antonio, M. R.; Soderholm, L. *Dalton Trans.* **2004**, 3562–3567.
(37) Fernandez, J. A.; Lopez, X.; Bo, C.; de Graaft, C.; Baerends, E. J.; Poblet, J. M. *J. Am. Chem. Soc.* **2007**, *129*, 12244–12253.
(38) Bartis, J.; Kunina, Y.; Blumenstein, M.; Francesconi, L. C. *Inorg. Chem.* **1996**, *35*, 1497–1501.
(39) Bartis, J.; Sukal, S.; Dankova, M.; Kraft, E.; Kronzon, R.; Blumenstein, M.; Francesconi, L. C. *Dalton Trans.* **1997**, 1937–1944.
(40) Luo, Q.;.; Howell, R. C.;.; Bartis, J.;.; Dankova, M.; Horrocks, W. D., Jr.; Rheingold, A. L.; Francesconi, L. C. *Inorg. Chem.* **2002**, *41*, 6112–6117.
(41) Lenoble, G.; Hasenknopf, B.; Thouvenot, R. *J. Am. Chem. Soc.* **2006**, *128*, 5735–5744.
(42) Kozik, M.; Baker, L. C. W. *J. Am. Chem. Soc.* **1990**, *112*, 7604–7611.
(43) Kozik, M.; Hammer, C. F.; Baker, L. C. W. *J. Am. Chem. Soc.* **1986**, *108*, 2748–2749.
(44) Contant, R.; Abbessi, M.; Canny, J.; Belhouari, A.; Keita, B.; Nadjo, L. *Inorg. Chem.* **1997**, *36*, 4961–4967.
(45) Contant, R.; Richet, M.; Lu, Y. W.; Keita, B.; Nadjo, L. *Inorg. Chem.* **2002**, 2587–2593.
(46) Keita, B.; Belhouari, A.; Nadjo, L.; Contant, R. *J. Electroanal. Chem.* **1998**, *442*, 49–57.
(47) Keita, B.; Girard, F.; Nadjo, L.; Contant, R.; Canny, J.; Richet, M. *J. Electroanal. Chem.* **1999**, *478*, 76–82.
(48) Keita, B.; Lu, Y. W.; Nadjo, L.; Contant, R. *Eur. J. Inorg. Chem.* **2000**, 2463–2471.
(49) Keita, B.; Mbomekalle, I. M.; Nadjo, L.; Contant, R. *Eur. J. Inorg. Chem.* **2002**, 473–479.

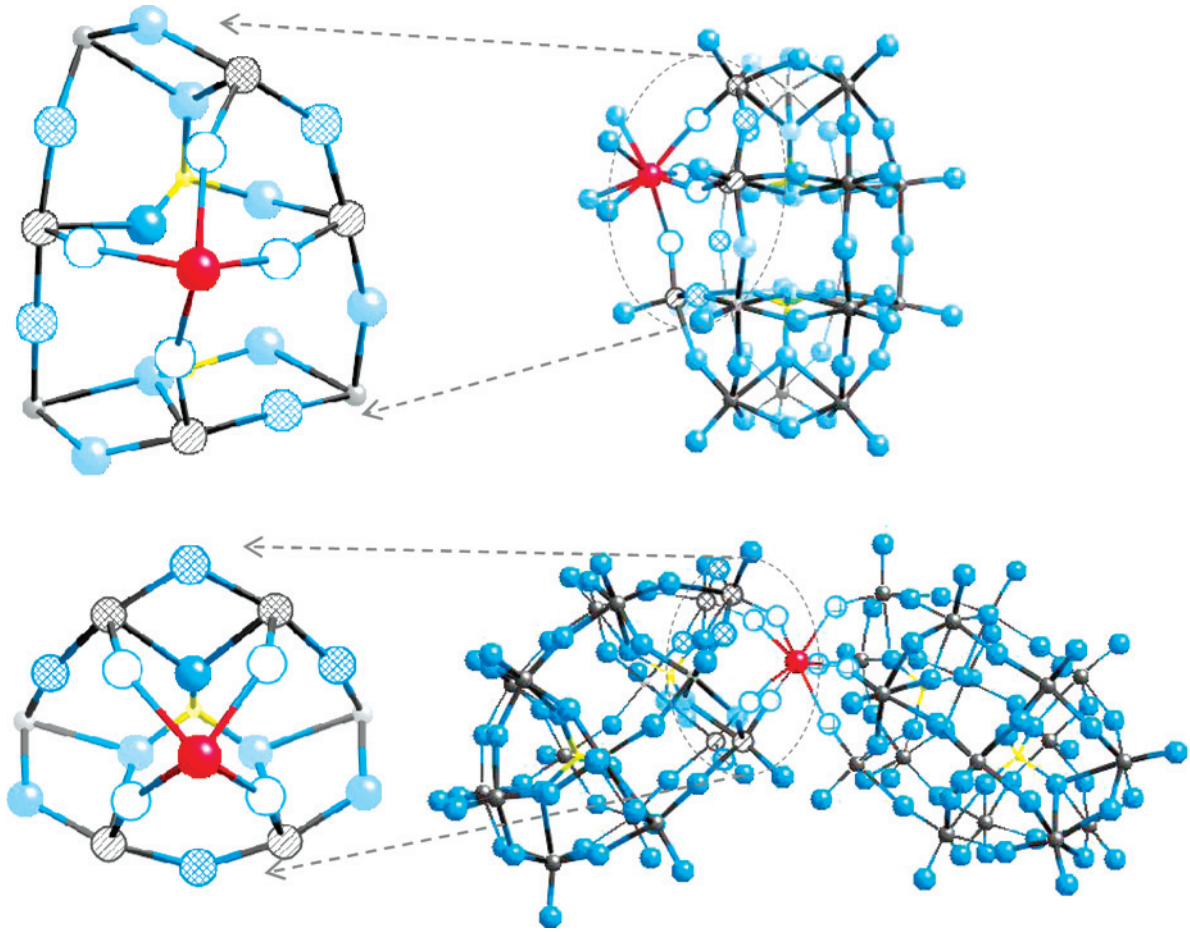

Figure 1. Local environments of Eu(III) (red spheres) in Eu-α-1 (top) and Eu-α-2 (bottom) showing the μ-O atom (open teal blue circles) connectivities with the W atoms in the belt, α-1 sites (striped black circles) and in the cap, α-2 sites (hatched black circles) of the tetradentate ligands.[46] In these two illustrations of the projected structures of 1:1 $[(H_2O)_4Eu(\alpha\text{-}1\text{-}P_2W_{17}O_{61})]^{7-}$ and 1:2 $[Eu(\alpha\text{-}2\text{-}P_2W_{17}O_{61})_2]^{17-}$, which are based upon the structures of the corresponding Lu(III) complexes,[62] the 4 terminal O atoms from H_2O molecules that complete the innermost Eu−O_8 coordination spheres are omitted for clarity, as are the majority of the atoms that constitute the framework structures. For the solid salt and solution of Eu-α-1 (top), the next-nearest interaction with the O atom (teal blue sphere) behind and to the left of the Eu ion as well as the more distant interactions with 4 W (3 striped and 1 hatched black circles) and 4 O (hatched teal blue circles) were refined in the EXAFS data. Phosphorus atoms are shown as yellow spheres.

with the W atoms in the belt (LUMO) of the α-1 ligand than in the α-2 ligand. The results from theoretical treatments, showing that the LUMO in the frontier molecular orbitals of $[\alpha\text{-}P_2W_{18}O_{62}]^{6-}$ consists of 96% α-1 character,[50–52] are consistent with experimental observations, including those showing that Eu(III) in an α-2 site, such as in $[Eu(\alpha\text{-}2\text{-}As_2W_{17}O_{61})_2]^{17-}$, is not reduced in an aqueous supporting electrolyte of 0.1 M CH_3CO_2Na + 0.1 M $NaClO_4$ at pH 5.0.[33,53]

The information about structural and electronic properties suggests to us that the $[\alpha\text{-}1\text{-}P_2W_{17}O_{61}]^{10-}$ lacunary POM would be an obvious system with which to deliberately couple Eu f states and POM-ligand d states by electrochemical means. In so doing, the reduction of Eu(III) in a complex molecular anion with dual centers of redox activity provides an opportunity for observation of correlated electron behaviors and otherwise interesting electrochemistry that would advance knowledge about the energetics of Eu-POMs, in general, and their applications in europium hydrometallurgy and electrocatalysis, in particular. The objective of this study is the investigation of the spectroscopy and electrochemistry for solutions of $K_7[(H_2O)_4Eu(\alpha\text{-}1\text{-}P_2W_{17}O_{61})]$ dissolved in aqueous electrolytes. Toward this end, we used the electrochemical techniques of cyclic voltammetry (CV) and bulk electrolysis (BE) as well as XAFS (X-ray absorption fine structure) spectroelectrochemistry. In particular, the Eu valence and coordination environment were probed through use of Eu L_3-edge XANES and EXAFS (extended X-ray absorption fine structure) obtained for the fully oxidized (colorless) complex anion, $[(H_2O)_4Eu(\alpha\text{-}1\text{-}P_2W_{17}O_{61})]^{7-}$, and for several multielectron reduced (heteropoly blue) forms, $[(H_2O)_4Eu(\alpha\text{-}1\text{-}P_2W_{17}O_{61})]^{n-}$, produced by exhaustive electrolysis at controlled electrode potentials simultaneously with the XAFS data acquisition. It is shown that Eu(III) in $[(H_2O)_4Eu(\alpha\text{-}1\text{-}P_2W_{17}O_{61})]^{7-}$ as dilute solutions (0.25 and 5.0 mM) in aqueous electrolytes of 0.2 M Li_2SO_4 at pH 3.0 is reduced to Eu(II) at sufficiently negative electrode potentials. The species containing Eu(II) and the reduced ligand is unstable with respect to autoxidation of Eu(II),

(50) Keita, B.; Jean, Y.; Levy, B.; Nadjo, L.; Contant, R. *New J. Chem.* **2002**, *26*, 1314–1319.
(51) Lopez, X.; Bo, C.; Poblet, J. M. *J. Am. Chem. Soc.* **2002**, *124*, 12574–12582.
(52) Lopez, X.; Bo, C.; Poblet, J. M. *Inorg. Chem.* **2003**, *42*, 2634–2638.
(53) Xi, X. D.; Wang, G.; Liu, B. F.; Dong, S. J. *Electrochim. Acta* **1995**, *40*, 1025–1029.

fragmentation, and rearrangement of the POM ligand, leading to the reconstitution of the plenary anion, $[\alpha\text{-}P_2W_{18}O_{62}]^{6-}$, and the formation of Eu(III) complexes of $[\alpha\text{-}2\text{-}P_2W_{17}O_{61}]^{10-}$ and $[PW_{11}O_{39}]^{7-}$ at negative electrode potentials. The mixed-solution speciation was confirmed by ^{31}P NMR spectroscopy and optical luminescence measurements.

Experimental Section

Solution and Sample Preparation. $K_7[(H_2O)_4Eu(\alpha\text{-}1\text{-}P_2W_{17}O_{61})]$, $K_7[(H_2O)_4Y(\alpha\text{-}1\text{-}P_2W_{17}O_{61})]$, $Al(H_3O)[(H_2O)_2Eu(PW_{11}O_{39})]$, $Cs_{11}[Eu(PW_{11}O_{39})_2]$, $K_7[Eu(\alpha\text{-}2\text{-}P_2W_{17}O_{61})]$, and $K_{17}[Eu(\alpha\text{-}2\text{-}P_2W_{17}O_{61})_2]$ were synthesized as previously described.[27,30,40] The plenary Wells−Dawson POM, $K_6[\alpha\text{-}P_2W_{18}O_{62}]$, and its lacunary, monovacant form, $K_9Li[\alpha\text{-}1\text{-}P_2W_{17}O_{61}]\cdot 20H_2O$, were prepared according to literature procedures.[54] $EuCl_3$, Eu_2O_3, YCl_3, and Li_2SO_4 were purchased from Aldrich Chemical Co. Aqueous supporting electrolyte solutions of 0.2 M Li_2SO_4 adjusted to pH 3.0 with H_2SO_4 (Fisher Optima) were used for all electrochemical and spectroscopic experiments in accordance with previous studies, showing that this medium imparts stability to metal complexes of $[\alpha\text{-}1\text{-}P_2W_{17}O_{61}]^{10-}$.[45] Indeed, we have found through the use of ^{31}P NMR that the stabilities of all fully oxidized Ln-POMs, $K_7[(H_2O)_4Ln(\alpha\text{-}1\text{-}P_2W_{17}O_{61})]$, in this aqueous supporting electrolyte are good (48 h before onset of decomposition). A solution of $Eu_2(SO_4)_3$ was prepared by dissolving Eu_2O_3 (9 mg) in the 0.2 M Li_2SO_4 solution electrolyte (10 mL). All chemical reagents were used as received. Deionized water (18 MΩ cm) was used for the preparation of all solutions.

^{31}P Nuclear Magnetic Resonance (NMR). ^{31}P NMR (161.8 MHz) spectra were recorded in 10 mm tubes with a volume of 3 mL on a JEOL GX-400 spectrometer. Typical acquisition parameters are as follows: spectral width, 10 000 Hz; acquisition time, 0.8 s; pulse delay, 1 s; pulse width, 15 μs (50° tip angle). Two-thousand scans were accumulated. A 85% H_3PO_4 solution was used as a chemical shift reference. The preparation of isomerically pure $K_7[(H_2O)_4Ln(\alpha\text{-}1\text{-}P_2W_{17}O_{61})]$ samples (5.0 mM) was established by their two-line spectra with δ(P1) and δ(P2) values of 6.42 and −11.41, −9.97 and −13.01 ppm for the complexes with Ln = Eu and Y, respectively. All chemical shifts are reported on the δ scale with upfield resonances as negative.

Electrochemical Measurements. A BAS 100B/W potentiostat (West Lafayette, IN) was used for the acquisition of all electroanalytical data, which were obtained from POM solutions (0.25 and 5.0 mM) at room temperature in 0.2 M Li_2SO_4 (pH 3.0). All reported potentials are given with respect to the Ag/AgCl reference electrode (BASi MF-2052). CV data for the lacunary ligand, $K_9Li[\alpha\text{-}1\text{-}P_2W_{17}O_{61}]$, its Ln complexes $K_7[(H_2O)_4Ln(\alpha\text{-}1\text{-}P_2W_{17}O_{61})]$ (Ln = Eu^{3+} and Y^{3+}), and $Eu(ClO_4)_3$ were obtained in one-compartment glass vials using a standard three-electrode system consisting of either glassy carbon (GC) (BASi MF-2012, geometrical area 0.071 cm^2) or 6.15 mm diameter graphite rod (GR) (Alfa 14739) working electrodes; 6.15 mm diameter GR auxiliary electrodes; the aforementioned Ag/AgCl reference electrodes. Each solution was deaerated with dinitrogen gas for 10−15 min prior to the CV measurement and subsequently blanketed with dinitrogen during all sweeps. Bulk electrolyses data for 5.0 mM solutions of $K_7[(H_2O)_4Ln(\alpha\text{-}1\text{-}P_2W_{17}O_{61})]$ (Ln = Eu and Y) were obtained in two-compartment electrochemical cell vials separated by a medium porosity glass frit to isolate the auxiliary and working GR electrodes. The solutions were step polarized from rest potential (+0.054 V) to an electrode potential of −1.30 V as they were vigorously sparged with dinitrogen throughout the course of exhaustive electrolysis, from which the net charge was used to calculate the number of electrons transferred per molecule through Faraday's law.

XAFS Data Acquisition and Analysis. Europium L_3-edge (6.977 keV) X-ray absorption spectroscopy (XAS) was performed at beamline 12-BM-B[55] at the Advanced Photon Source. The incident X-ray energy was calibrated by the first inflection point energy for the K-edge XANES of iron foil, 7.112 keV. All of the measurements were made in the fluorescence mode at ambient conditions with a multielement (Canberra) detector. The neat powder of $K_7[(H_2O)_4Eu(\alpha\text{-}1\text{-}P_2W_{17}O_{61})]$ was pressed into a micro X-ray cell (SPEX 3577) with Prolene X-ray film windows (4 μm gauge, Chemplex Industries), and its solutions of 0.25 mM and 5.0 mM POM concentrations (5 mL in 0.2 M Li_2SO_4 electrolyte, pH 3.0) were injected into purpose-built electrochemical cells for measurement.[56,57] The data from three one-hour scans of the white powder sample and the 5.0 mM solution (in its colorless-oxidized state as well as the blue-reduced form) were averaged for analysis of EXAFS, which was performed in consistent fashion in the usual manner[58] with *EXAFSPAK*[59] and *WinXAS 3.1*,[60] and theoretical phase and amplitude functions were calculated with *FEFF 8.0*.[61] Conventional metrical treatments of the Eu $k^3\chi(k)$ EXAFS with a fixed-scale factor ($S_0^2 = 0.9$) entailed a series of stepwise fits of increasing complexity, from single- to multishell coordination models based upon the crystallographic data available for the structure of the corresponding lutetium POM, $[(H_2O)_4Lu(\alpha\text{-}1\text{-}P_2W_{17}O_{61})]^{7-}$.[62] Ultimately, the EXAFS spectra were precisely modeled with either three- or four-shell fits that included contributions from the nearest O atoms as well as the distant neighbors of O, P, and W. The number of refined parameters (10) was less than the number of relevant independent data points, $N_I = 16$, available in the primary spectra, with $k_{max} = 10.2$ Å^{-1} and $\Delta r = 3$ Å.[63] The in situ X-ray absorption spectroelectrochemical data were collected on the deaerated and continuously N_2-sparged solution of the fully oxidized $[(H_2O)_4Eu(III)(\alpha\text{-}1\text{-}P_2W_{17}O_{61})]^{7-}$ anion in the aqueous electrolyte at the electrode open circuit potential, +0.054 V. This was followed by bulk electrolysis at −1.30 V and at −0.90 V for the concentrated (5.0 mM) and dilute (0.25 mM) solutions, respectively, of $[(H_2O)_4Eu(III)(\alpha\text{-}1\text{-}P_2W_{17}O_{61})]^{7-}$ to produce the corresponding reduced anions containing Eu(II). XANES data were recorded with respect to time, while electrode polarization was maintained to probe the stability of the reduced species. The time-dependent spectra obtained at each electrode potential were fit using linear combination analyses with the end member spectra for the oxidized, Eu(III), and reduced, Eu(II), POMs as well as with pseudo-Voigt and arctangent functions.

(54) Contant, R. *Inorganic Syntheses*; Ginsberg, A. P., Ed.; Wiley-Interscience: New York, 1990; Vol. 27; pp 104−107.

(55) Beno, M. A.; Engbretson, M.; Jennings, G.; Knapp, G. S.; Linton, J.; Kurtz, C.; Rütt, U.; Montano, P. A. *Nucl. Instrum. Methods Phys. Res., Sect. A* **2001**, *467−468*, 699–702.

(56) Soderholm, L.; Antonio, M. R.; Williams, C.; Wasserman, S. R. *Anal. Chem.* **1999**, *71*, 4622–4628.

(57) Antonio, M. R.; Soderholm, L.; Song, I. *J. Appl. Electrochem.* **1997**, *27*, 784–792.

(58) Gannaz, B.; Antonio, M. R.; Chiarizia, R.; Hill, C.; Cote, G. *Dalton Trans.* **2006**, 4553–4562.

(59) George, G. N.; Hilton, J.; Temple, C.; Prince, R. C.; Rajagopalan, K. V. *J. Am. Chem. Soc.* **1999**, *121*, 1256–1266.

(60) Ressler, T. *J. Phys. IV* **1997**, *7*, 269–270.

(61) Rehr, J. J.; Albers, R. C. *Rev. Mod. Phys.* **2000**, *72*, 621–654.

(62) Luo, Q. H.; Howell, R. C.; Dankova, M.; Bartis, J.; Williams, C. W.; Horrocks, W. D.; Young, V. G.; Rheingold, A. L.; Francesconi, L. C.; Antonio, M. R. *Inorg. Chem.* **2001**, *40*, 1894–1901.

(63) Stern, E. A. *Phys. Rev. B* **1993**, *48*, 9825–9827.

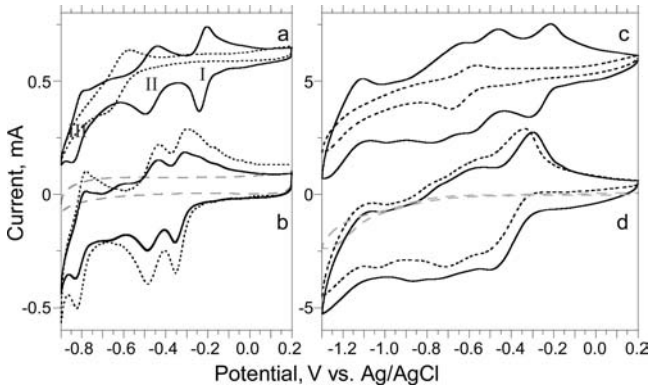

Figure 2. Cyclic voltammograms, $\nu = 49$ mV s^{-1}, of 0.25 mM (left panel) and 5.0 mM (right panel) analytes (a, c) $[\alpha\text{-}1\text{-}P_2W_{17}O_{61}]^{10-}$ (solid line) and $Eu(ClO_4)_3$ (dashed line: left panel 1.0 mM, right panel 5.0 mM)); (b, d) background scan (gray dashed line), Eu-α-1 (solid line), and Y-α-1 (black dashed line) on GR electrodes in 0.2 M Li_2SO_4 electrolyte at pH 3.0. The data in parts a and c are offset for clarity.

Optical Luminescence. $K_7[(H_2O)_4Eu(\alpha\text{-}1\text{-}P_2W_{17}O_{61})]$ (0.233 g, 46.6 μmol) was dissolved in 10 mL Li_2SO_4 (0.2 M, pH 3.0) and placed in an electrochemical cell. The solution was reduced at a potential of −1.30 V for 4 h under an atmosphere of dinitrogen. An aliquot of this reduced solution was taken for analysis (200 μL in 2000 μL Li_2SO_4 buffer, 0.466 mM).

The remaining solution was oxidized at a potential of +1.00 V for 5 h (until the solution was completely clear) and a sample was taken for the final spectroscopic analysis. Standard solutions of $K_7[Eu(\alpha\text{-}2\text{-}P_2W_{17}O_{61})]$, $K_{17}[Eu(\alpha\text{-}2\text{-}P_2W_{17}O_{61})_2]$, $Al(H_3O)[(H_2O)_2Eu(PW_{11}O_{39})]$, $Cs_{11}[Eu(PW_{11}O_{39})_2]$, and $Eu_2[SO_4]_3$ were prepared at a working concentration of ∼0.5 mM also in Li_2SO_4 (0.2 M, pH 3.0) and placed in quartz cuvettes for analyses. Eu(III) excitation spectra and excited-state lifetimes were obtained using a Spectra-Physics Quanta Ray PRO-270−10 Q-switched Nd:YAG pump laser (10 Hz, 60−70 mJ/pulse) and a MOPO SL for all luminescence measurements as reported.[64] The nondegenerate $^7F_0 \rightarrow {}^5D_0$ transition of the Eu(III) ion was scanned between 578 and 582 nm, whereas the $^5D_0 \rightarrow {}^7F_2$ emission band was monitored at 614 nm. Excitation spectra were deconvoluted by using the program *PeakFit 4.12* (Jandel). Time-resolved luminescence measurements were collected by using a digital Tektronix TDS 3034B oscilloscope. Data were fit to single and double exponential decays by using *Sigmaplot* version 10 (Systat).

Results and Discussion

Electrochemical Studies. Cyclic voltammograms obtained for two concentrations — 0.25 and 5.0 mM — of three analytes — $[\alpha\text{-}1\text{-}P_2W_{17}O_{61}]^{10-}$, $[Eu(\alpha\text{-}1\text{-}P_2W_{17}O_{61})]^{7-}$, and $[Y(\alpha\text{-}1\text{-}P_2W_{17}O_{61})]^{7-}$ (abbreviated hereafter as α-1, Eu-α-1, and Y-α-1, respectively) — and two concentrations — 1.0 and 5.0 mM — of Eu(III) in the pH 3.0 aqueous electrolyte of 0.2 M Li_2SO_4 are shown in Figure 2. The data of part a of Figure 2 (solid black line) for the 0.25 mM Ln-free lacunary anion shows three well-resolved processes with $E_{1/2}$ = −0.22, −0.47, and −0.81 V (identified as I, II, and III), which are attributed to W-based redox chemistry involving three successive two-electron couples.[65] The response is essentially the same as reported beforehand for 0.25−0.5 mM solutions of $K_9Li[\alpha\text{-}1\text{-}P_2W_{17}O_{61}]$ in 0.2 M Na_2SO_4 aqueous electrolytes of pH 3.0.[45–47] Repetitive sweeps between −0.90 and +0.20 V showed reproducible behavior even though the original, colorless solution changed to light blue during the course of experimentation with different scan rates (Figure S0, Supporting Information). The blue color arises from the reductive electrochemistry and delocalization of the added electrons in the LUMOs that consist of W (α-1, belt site of Figure 1, left) and O character.[66–69]

Table 1. Peak Potentials (±0.005 V) for the Redox Couples Observed in the Cyclic Voltammograms of Figure 2[a]

anion	wave	E_{pc}[V][b]	E_{pa}[V][c]	$E_{1/2}$[V][d]	ΔE_p[V][e]
		0.25 mM			
$[\alpha\text{-}1\text{-}P_2W_{17}O_{61}]^{10-}$	I	−0.241	−0.204	−0.223	0.037
	II	−0.502	−0.436	−0.469	0.066
	III	−0.836	−0.783	−0.810	0.053
Y-α-1	I	−0.354	−0.298	−0.326	0.056
	II	−0.485	−0.431	−0.458	0.054
	III	−0.825	−0.780	−0.803	0.045
Eu-α-1	I	−0.356	−0.311	−0.334	0.045
	II	−0.487	−0.436	−0.462	0.051
	III	−0.675	−0.617	−0.646	0.058
	IV	−0.831	−0.782	−0.807	0.049
$Eu(ClO_4)_3$	I	−0.677	−0.572	−0.625	0.105
		5.0 mM			
$[\alpha\text{-}1\text{-}P_2W_{17}O_{61}]^{10-}$	I	−0.32	−0.22	−0.27	0.10
Y-α-1	I	−0.49	−0.34	−0.42	0.15
Eu-α-1	I	−0.50	−0.30	−0.40	0.20
$Eu(ClO_4)_3$	I	−0.69	−0.57	−0.63	0.12

[a] Left panel: For 0.25 mM $[\alpha\text{-}1\text{-}P_2W_{17}O_{61}]^{10-}$, Y-α-1, Eu-α-1, and 1.0 mM for $Eu(ClO_4)_3$ on GR working electrodes at 49 mV s^{-1}. The right panel gives the peak potentials (±0.01 V) for the first couple (I) in the CV data for the 5.0 mM analytes. [b] E_{pc} is the electrode potential of peaks with cathodic current. [c] E_{pa} is the electrode potential of peaks with anodic current. [d] $E_{1/2} = (E_{pc} + E_{pa})/2$. [e] $\Delta E_p = E_{pa} - E_{pc}$.

The data in part a of Figure 2 (black dashed line) for a 1.0 mM Eu(III) solution shows a single process with $E_{1/2}$ = −0.63 V, which is attributed to the one-electron Eu(III)/Eu(II) couple. The standard electrode potential for this process is −0.55 V versus Ag/AgCl.[70] The more-negative experimental value is attributed to stabilizing effects of sulfate complexation with Eu(III) in much the same manner as the electrode potential of the Ce(III)/Ce(IV) couple is lowered by complexation with $[SO_4]^{2-}$.[71] Of essence here is that the Eu redox activity occurs within the electrode potential region for the ligand-centered reduction of the W−O POM framework alone. As such, the CV data for Eu-α-1 shown in part b of Figure 2 (solid black line) may be an amalgamation of Eu- and ligand-centered redox activities. The values of $E_{1/2}$ for the 4 redox couples are provided in Table 1. These show that Eu(III) complexation with $[\alpha\text{-}1\text{-}P_2W_{17}O_{61}]^{10-}$ results in a negative shift of 0.11 V of the first redox couple, I, equivalent to the effects observed upon transition-metal-ion complexation with α-1.[47] The second

(64) Nwe, K.; Richard, J. P.; Morrow, J. R. *Dalton Trans.* **2007**, 5171–5178.
(65) Contant, R.; Ciabrini, J. P. J. *Chem. Res.* **1977**, 222.
(66) Pope, M. T. In *Mixed-Valence Compounds. Theory and Applications in Chemistry, Physics, Geology, and Biology*; Brown, D. B., Ed.; D. Reidel: Dordrecht, 1980; pp 365−386.
(67) Papaconstantinou, E.; Pope, M. T. *Inorg. Chem.* **1970**, *9*, 667–669.
(68) Varga, G. M., Jr.; Papaconstantinou, E.; Pope, M. T. *Inorg. Chem.* **1970**, *9*, 662–667.
(69) Pope, M. T.; Papaconstantinou, E. *Inorg. Chem.* **1967**, *6*, 1147–1152.
(70) Bratsch, S. G. *J. Phys. Chem. Ref. Data* **1989**, *18*, 1–21.
(71) Wadsworth, E.; Duke, F. R.; Goetz, C. A. *Anal. Chem.* **1957**, *29*, 1824–1825.

and the third couples of the anionic ligand alone (II and III, respectively, in Table 1) are effectively preserved in the response of Eu-α-1 as couples II and IV. The principal variation between the ligand and Eu-α-1 is the presence of a new feature at $E_{1/2} = -0.65$ V, which is nearly coincident with the response of free Eu and with a peak separation, ΔE_p, of 0.058 V, indicating one-electron Eu(III)/Eu(II) redox activity in Eu-α-1. The presumed mixing of Eu- and W-centered electrochemical processes in the complex anion parallels the heterobinuclear reductive response of Fe(III) and α-1 in the Fe(III)-α-1 system.[46]

To provide insight into this issue, the CV data for a 0.25 mM solution of Y-α-1 was recorded and is shown in part b of Figure 2 as the black dashed line. Because Y(III) is not reducible to Y(II) in aqueous electrolytes, the electrochemical response will be that of the ligand alone as modified by Y(III) complexation, so a difference between Y-α-1 and Eu-α-1 stands to be an indicator of Eu redox activity. Three couples are evident for Y-α-1 with $E_{1/2}$ values (I−III, Table 1) that are in agreement with three of the four processes observed for Eu-α-1. This comparison indicates that waves I, II, and IV of Eu-α-1 are attributable to W electrochemistry. Couple III at $E_{1/2} = -0.65$ V is unique to Eu-α-1 — there is no wave between −0.60 and −0.70 V in the CV for Y-α-1 — and is evidence to support the assignment of Eu redox activity in the bulk voltammetric response for Eu-α-1. Confirmation of the Eu valence switching is provided through use of XANES spectroelectrochemisty, vide infra.

The CV data for the 5.0 mM solution analyte concentrations are shown in parts c and d of Figure 2 in identical fashion to the presentation of the data for the 0.25 mM analytes of parts a and b of Figure 2. In comparing the CVs in the left and right panels of Figure 2, two differences are obvious vis-à-vis the negative electrode potential switching limits and the current response itself. The negative limits of −0.90 and −1.30 V for the 0.25 and 5.0 mM analyte concentrations, respectively, are determined by the onset of the hydrogen evolution reaction, which appears to be promoted by surface derivatization by the analytes at low concentrations in the acidic medium.[72] The rather dramatic and detrimental changes of appearance, in terms of peak broadening and poor peak separations, for the CVs obtained at the high (5.0 mM) POM concentrations are indicators of, in part, solvent and solute effects, especially interion-associations, such as have become commonplace in organic[73–75] and aqueous[76–80] POM electrochemistry. Nevertheless, in considering the first redox couple, which is the only one with clear resolution even in the corresponding semidifferential data (Figure S1, Supporting Information), the trends in the $E_{1/2}$ values for the 0.25 mM analytes are consistent with the 5.0 mM solutions (Table 1). In particular, the couples for Eu-α-1 and Y-α-1 are 0.13−0.15 V less than that for the ligand itself. Whereas there are subtle differences between the data for Y-α-1 and Eu-α-1, shown in part d of Figure 2, it is not possible to disentangle the ligand, W-centered processes from one for the Eu(III)/Eu(II) couple, as was possible with the CV data for 0.25 mM Eu-α-1 (part b of Figure 2). The same systematic comparison of the CV data for the 5.0 mM α-1 and Ln-α-1 POMs reveals complicated behaviors that may arise from combined effects of interion associations, polydispersity, protonation, isomerization, analyte instabilities, and so forth. For instance, although the $E_{1/2}$ values for the 5.0 mM analytes are slightly (0.005−0.09 V) more negative than the corresponding values obtained at 0.25 mM, the ΔE_p values for the 5.0 mM analytes at 49 mV s^{-1} are large, 0.10−0.20 V, (Table 1) and significantly (1.8−5.4 ×) greater than those for the 0.25 mM analytes at the same scan rate. This suggests that the electron transfer kinetics are slower for the species in the concentrated analytes than for those in the dilute ones.

Information about the redox kinetics of α-1 and Ln-α-1 at the GR electrode surface is provided by plots of the peak currents for the cathodic and anodic processes of couple I (i_{pc} and i_{pa}, respectively) versus the square roots of the scan rates, $\nu^{1/2}$. Figure 3 shows that a linear proportionality exists between the currents and $\nu^{1/2}$ for both analyte concentrations — 0.25 (a, b) and 5.0 (c, d) mM. The primary data (shown as symbols) are adequately described by the linear fits ($R^2 = 0.86-0.99$, shown as lines) with intercepts of zero according to the Randles−Sevcik equation, indicating that the electron transfer kinetics are mass-transport controlled.[81] The individual slopes and regressions coefficients, tabulated in the Supporting Information (Table S0), show that the ratio of average peak currents, i_{pa}/i_{pc}, is less than unity (0.8−0.9) for the dilute, 0.25 mM analyte concentrations and is greater than unity (1.1−1.6) for the 5.0 mM analyte concentrations for all 4 scan rates, 9, 25, 49, and 100 mV s^{-1}. These deviations indicate irreversible behaviors, which are corroborated by the plots of ΔE_p versus ν, showing (Figure S2, Supporting Information) that the peak potential separations increase with increasing scan rates for both the 0.25 and 5.0 mM analyte concentrations and, consequently, that electron transfer kinetics are slow relative to the aforementioned scan rates. The combined deviations of peak currents and potentials from ideal, Randles−Sevcik, and Nernst behaviors suggest electrochemical irreversibilities, such as may result from redox processes that are coupled to chemical reactions involving the electrolyzed species, may also be at play.

We sought to obtain additional information about the electrochemical processes by use of controlled potential

(72) Keita, B.; Nadjo, L. *Mater. Chem. Phys.* **1989**, *22*, 77–103.
(73) Maeda, K.; Katano, H.; Osakai, T.; Himeno, S.; Saito, A. *J. Electroanal. Chem.* **1995**, *389*, 167–173.
(74) Osakai, T.; Katano, H.; Maeda, K.; Himeno, S.; Saito, A. *Bull. Chem. Soc. Jpn.* **1993**, *66*, 1111–1115.
(75) Osakai, T.; Maeda, K.; Ebina, K.; Hayamizu, H.; Hoshino, M.; Muto, K.; Himeno, S. *Bull. Chem. Soc. Jpn.* **1997**, *70*, 2473–2481.
(76) Grigoriev, V. A.; Cheng, D.; Hill, C. L.; Weinstock, I. A. *J. Am. Chem. Soc.* **2001**, *123*, 5292–5307.
(77) Grigoriev, V. A.; Hill, C. L.; Weinstock, I. A. *J. Am. Chem. Soc.* **2000**, *122*, 3544–3545.
(78) López, X.; Nieto-Draghi, C.; Bo, C.; Avalos, J. B.; Poblet, J. M. *J. Phys. Chem. A* **2005**, *109*, 1216–1222.
(79) Toth, J. E.; Anson, F. C. *J. Electroanal. Chem.* **1988**, *256*, 361–370.
(80) Weinstock, I. A.; Grigoriev, V. A.; Cheng, D.; Hill, C. L. In *Polyoxometalate Chemistry for Nano-Composite Design*; Yamase, T., Pope, M. T., Eds.; Kluwer: New York, 2002; pp 103−127.
(81) Bard, A. J.; Faulkner, L. R. *Electrochemical Methods: Fundamentals and Applications*, 2nd ed.; J. Wiley: New York, 2001.

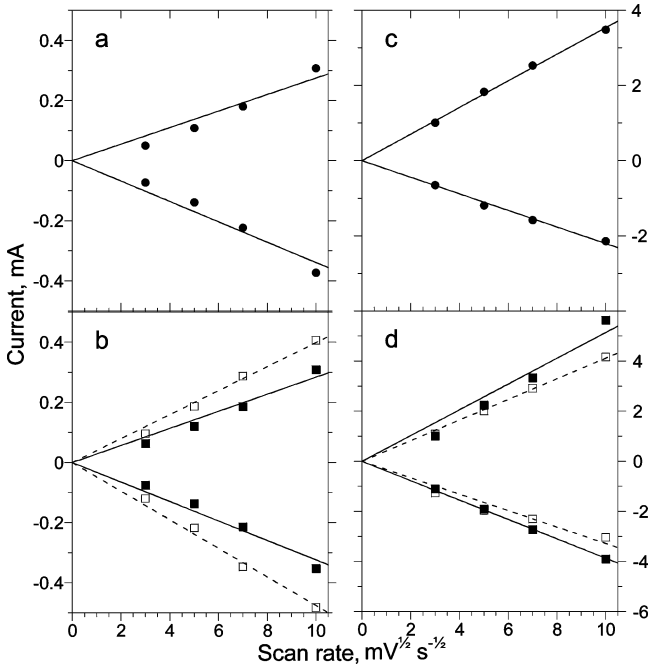

Figure 3. Anodic and cathodic peak current, i_{pa} and i_{pc}, variations of the first redox couple (I, Table 1) with the square roots of scan rates from CVs of 0.25 mM (left panel) and 5.0 mM (right panel) analytes (a, c) $[\alpha\text{-}1\text{-}P_2W_{17}O_{61}]^{10-}$; (b, d) Eu-α-1 (solid squares and solid lines) and Y-α-1 (open squares and dashed lines) on GR electrodes in 0.2 M Li_2SO_4 electrolyte at pH 3.0 and ν = 9, 25, 49, and 100 mV s^{-1} (Supporting Information). The fitted lines are based upon the Randles−Sevcik equation, $i_p = (5.02RT)^{-1/2}(nF)^{3/2}ACD^{1/2}\nu^{1/2}$ with the conventional symbol meanings.[81] All slopes, which are negative for the i_{pc} response and positive for i_{pa}, and regression coefficients are provided as Supporting Information, Table S0.

electrolysis of fully oxidized α-1 and Ln-α-1 POM solutions. In agreement with the literature,[47,65] a 5.0 mM solution of the α-1 ligand was found to consume 6.1 electrons per molecule upon exhaustive electrolysis at −1.30 V. The comparable experiments with 5.0 mM and 0.25 mM solutions of Eu-α-1 and Y-α-1 were less conclusive. The results show the transfer of 5.8−10.2 electrons for Eu-α-1 and 6.0−7.9 electrons for Y-α-1. We attribute this unusually high dispersion of results from repeated measurements performed under identical conditions to interferences from chemical reactions, particularly those resulting from the reactivity of the reduced Ln-α-1 complexes toward isomerization and rearrangement, forming electroactive species in addition to Ln-α-1. As pointed out beforehand,[46] such chemical interferences in the labile α-1 system can complicate the overall count of charge (electrons) consumed throughout the time scale of a bulk electrolysis experiment. Whereas the results from BE are inconclusive regarding evidence about Eu redox activity in Eu-α-1, as indicated by the CV measurements of the 0.25 mM analyte and its structural chemistry, direct and definitive insights about both issues were obtained by the use of in situ Eu XAFS.

Eu L_3-edge XAFS. Spectra were first acquired for the solid salt of Eu-α-1 and for a freshly prepared 5.0 mM solution of it in fully oxidized form at rest potential (+0.054 V) to confirm that the coordination environment about Eu(III) in the solid state does not change upon dissolution in the 0.2 M Li_2SO_4 electrolyte. The XANES and EXAFS data are

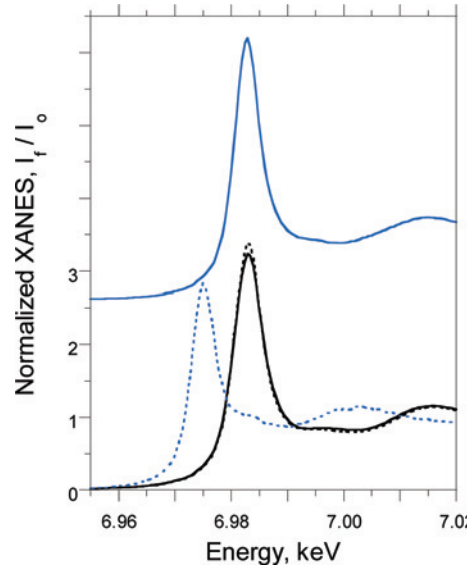

Figure 4. Normalized Eu L_3-edge XANES spectra of Eu-α-1 solid salt (solid black line) and its freshly prepared, fully oxidized 5.0 mM Eu-α-1 solution at rest potential, +0.054 V (dashed black line), in the in 0.2 M Li_2SO_4 electrolyte of pH = 3.0; reduced, heteropoly blue solution with the GR electrode polarized at −1.30 V (dashed blue line); and after oxidation at −1.00 V (solid blue line, offset for clarity). The Eu(III) edge peaks at 6.9829 keV have a fwhm of 6.4 eV, and the Eu(II) edge peak at 6.9749 keV has a fwhm of 5.0 eV, consistent with the inverse relationship between line width and IR.[57]

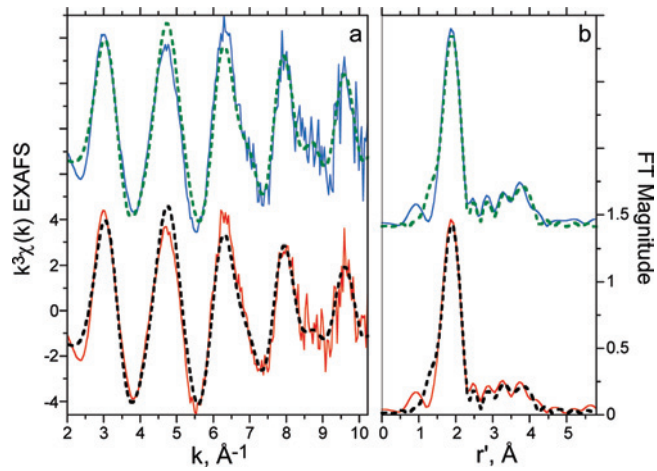

Figure 5. Eu L_3-edge $k^3\chi(k)$ EXAFS data (a) and corresponding Fourier transform data (b) for Eu-α-1 solid salt (top, offset for clarity) and its freshly prepared, fully oxidized 5.0 mM Eu-α-1 solution at rest potential, +0.054 V, (bottom) as described in Figure 4. The solid lines illustrate the experimental data, and the dashed lines show the fits.

shown as Figures 4 and 5, respectfully. The intense edge peaks at 6.9829 keV observed in the XANES are characteristic of Eu(III),[57,62,82] and the coincident responses suggest that the Eu coordination for the solution species is stable and equivalent to that of the solid. The experimental $k^3\chi(k)$ EXAFS and the corresponding Fourier transform (FT) data of Figure 5 (without phase correction) confirm the structural identity. In the absence of single-crystal X-ray diffraction data for Eu-α-1, the fitting of the primary Eu EXAFS (solid lines) was modeled upon the known structure of $K_7[(H_2O)_4\text{-}Lu(\alpha\text{-}1\text{-}P_2W_{17}O_{61})]$ (abbreviated hereafter as Lu-α-1), which shows that Lu(III) is 8-coordinated with O atoms at an average distance of 2.36(6) Å.[62] The average bond length

between Lu and the four O atoms of the tetradentate α-1 ligand is 2.30(4) Å. The square antiprism of O around Lu(III) is completed by complexation of four water molecules with an average distance of 2.42(5) Å. Our Eu EXAFS is of insufficient resolution ($\Delta k = 8.2$ Å^{-1}; $\Delta r = 0.19$ Å) to show two separate O peaks in the FT data, which instead reveal a single intense peak at 1.86 Å (before phase shift, part b of Figure 5) containing the combined O backscattering contributions.

The EXAFS for the solid salt and aqueous solution of Eu-α-1 were fit to reveal 7.6 ± 1 nearest O at 2.37(1) Å and 7.8 ± 1 O at 2.38(1) Å, respectively. The O coordination numbers (CNs) agree with those obtained for the solid salt of Lu-α-1 (8) and for an aqueous solution of Eu-α-1 (7.8). The latter value was obtained as the sum of 4 O, from the α-1 ligand, and 3.8 bound H_2O, as determined from luminescence lifetimes of Eu-α-1 measured in H_2O and D_2O.[30] The EXAFS results for the solid and solution of Eu-α-1 are in agreement with the 1:1 formulation of the $[(H_2O)_4Eu(\alpha\text{-}1\text{-}P_2W_{17}O_{61})]^{7-}$ complex, wherein Eu(III) binds to four O atoms of the POM ligand and four other coordination sites are occupied by water molecules, possibly with the stereochemistry that obtains for the Lu-α-1 crystal structure. The fact that the average Eu−O distances, 2.37−2.38 Å, are only 0.01−0.02 Å longer than the average Lu−O distance is unexpected in view of the 0.089 Å larger ionic radius for Eu(III), 1.066 Å, versus Lu(III), 0.977Å, for CN = VIII.[83]

Additional evidence that the Eu-α-1 molecular complex remains stable and intact upon dissolution of the solid and throughout the course of the measurements is provided by the analysis of the three distant peaks — 2.86, 3.26, and 3.72 Å — in the FT data of part b of Figure 5. The fits (shown as dashed lines in Figure 5) to the Eu EXAFS data of the solid and solution samples obtained from the 4-shell model with fixed CNs for the distant interactions based upon the Lu-α-1 environment are convincing. The three small peaks correspond to backscattering from one O at 3.36−3.37 Å, four W at 3.74 Å, and four O at 4.37−4.39 Å. The complete metrical parameters are provided in Table 2. These distances compare favorably with those — 3.41(1), 3.97(8), and 4.33(9) Å, respectively — from the X-ray crystallographic investigation of the Lu-α-1 system.[62]

Following acquisition of the solution EXAFS for the oxidized Eu-α-1 at the rest potential described above, the electrode potential was step polarized to −1.30 V to produce the reduced species. Upon achieving exhaustive electrolysis after 125 min, the Eu L_3-edge XANES of Figure 4 (blue dashed line) for the heteropoly blue, reduced analyte reveals a new edge peak at 6.9749 keV, approximately 8 eV below the Eu(III) peak for the oxidized analyte, that is diagnostic of Eu(II).[57,84,85] This in situ XANES spectroelectrochemistry experiment provides direct confirmation of the independent results from CV alone, vide supra, by demonstrating that

Table 2. Results of Curve-Fitting Analysis of the Eu L_3-edge $k^3\chi(k)$ EXAFS of Figures 5 and 7[a]

sample	shell	CN[b]	r,[c] Å	σ^2,[d] Å^2	ΔE_0[e]
solid salt Eu-α-1	Eu−O	7.6(10)	2.37(1)	0.009(2)	−0.2
	Eu−O	1	3.36(7)	0.004(9)	[f]
	Eu−W	4	3.74(2)	0.009(3)	[f]
	Eu−O	4	4.4(1)	0.008(9)	[f]
original Eu-α-1	Eu−O	7.8(10)	2.38(1)	0.009(2)	−0.03
solution	Eu−O	1	3.37(9)	0.008(12)	[f]
	Eu−W	4	3.74(2)	0.011(3)	[f]
	Eu−O	4	4.4 (1)	0.02(2)	[f]
oxidized Eu-α-1	Eu−O	9.0(10)	2.42(2)	0.012(3)	1.4
solution obtained	Eu−P	3.9(9)	3.16(3)	0.013(9)	[f]
after reduction	Eu−P	1.8(8)	4.15(3)	0.001(9)	[f]

[a] The number in the parentheses represents the estimated standard deviations (3σ) obtained from the least-squares fits. [b] Coordination number. [c] Interatomic distance. [d] The Debye−Waller factor, the root-mean-square deviation of the average Eu−X bond length, for X = O, P, W. [e] The energy difference between the experimental and theoretical values of E_0. [f] Parameter fixed to the value in the column above.

Eu(III) is, indeed, reduced along with the P−W−O ligand. With the possible exception of $[Eu(III)(W_5O_{18})_2]^{9-}$,[86] it is only the second known example of such behavior in Eu-POMs, the first being the Eu(III)-Preyssler POM.[32]

During the subsequent campaign to obtain high-quality EXAFS for the pure Eu(II)-α-1 solution species, we observed an autoxidation process — with the electrode continuously polarized at −1.30 V — commencing some 15 min after producing the Eu(II) solution species. The XANES data of part a of Figure 6 show the time evolution of the autoxidation to Eu(III). This dynamic behavior demonstrates that the electrochemical interconversion between the fully oxidized Eu(III)-α-1 anion and its multielectron-reduced species, Eu(II)-α-1, is an irreversible, non-Nernstian process. The EXAFS data obtained within the ca. 50 min time frame (110−160 min, part b of Figure 6) when there is ≤5% of the autooxidized Eu(III) species formed were analyzed in terms of its Eu−O bonding. A single-shell fit to the data for the metastable, reduced POM indicates that there are 7.7 ± 1.0 O atoms about Eu(II) with an average distance of 2.55(4) Å (Supporting Information, Figure S3). This bond length is 0.17 Å longer than that (2.38(1) Å) for the original solution of Eu(III)-α-1. The increase is consistent with the 0.184 Å larger IR of Eu(II), which is 1.25 Å for CN = VIII, versus Eu(III).

The in situ Eu XANES acquired following exhaustive electrolysis of the fully oxidized, dilute (0.25) mM Eu-α-1 solution with the electrode polarized at −0.90 V confirms the response observed with the 5.0 mM analyte. That is, the reduced Eu(II)-α-1 anion is a labile species prone to autoxidation and structural transformations, which were addressed by subsequent experimentation described here. Some 30% of the fully reduced Eu(II)-α-1 species in the 5.0 mM analyte is autoxidized to Eu(III) after 6.7 h with the electrode at −1.30 V (part b of Figure 6). To accelerate the oxidation of the remaining Eu(II), the solution was

(82) Rohler, J. In *Handbook on the Physics and Chemistry of Rare Earths*; Gschneidner, K. A., Jr., Eyring, L., Hufner, S., Ed.; North-Holland: Amsterdam, 1987; Vol. 10 - High Energy Spectroscopy; pp 453−545.
(83) Shannon, R. D. *Acta Crystallogr., Sect. A* **1976**, *32*, 751–767.
(84) Moreau, G.; Helm, L.; Purans, J.; Merbach, A. E. *J. Phys. Chem. A* **2002**, *106*, 3034–3043.
(85) Rakovan, J.; Newville, M.; Sutton, S. *Am. Mineral.* **2001**, *86*, 697–700.
(86) Mulazzani, Q. G.; Venturi, M.; Ballardini, R.; Gandolfi, M. T.; Balzani, V. *Isr. J. Chem.* **1985**, *25*, 183–188.

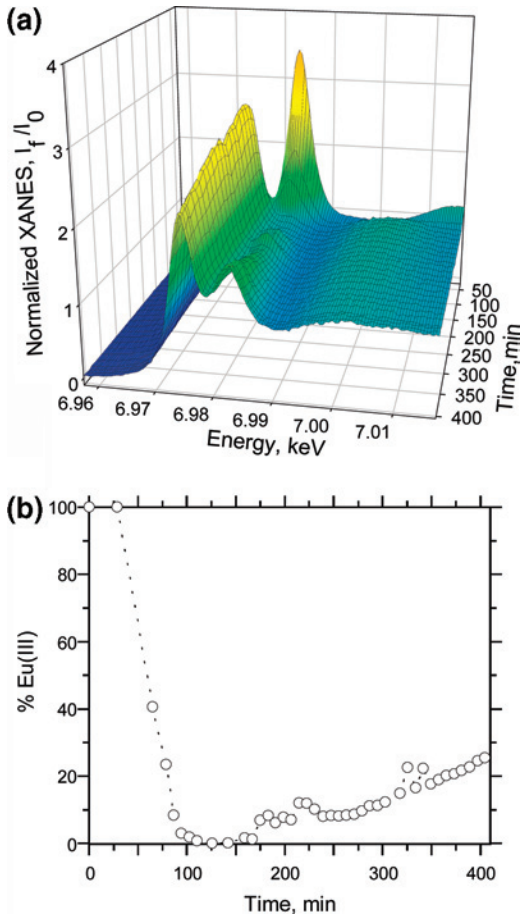

Figure 6. (a) Normalized Eu L_3-edge XANES for the 5.0 mM Eu-α-1 solution from one hour after starting electrode polarization at −1.30 V to the final scan some 7 h later, showing the initial reduction of Eu(III) and the subsequent autoxidation of Eu(II) while under potential control. (b) Time evolution of the Eu(III) valence in Eu-α-1 throughout the bulk electrolysis experiment of part (a).

electrolyzed with an electrode potential of −1.00 V. The Eu XANES obtained for the heteropoly blue solution following exhaustive electrolysis, Figure 4 (blue solid line), shows the presence of only Eu(III), confirming the complete oxidation of Eu(II). The corresponding EXAFS and FT data of the blue, Eu(III) solution maintained at −1.00 V are shown in Figure 7. This FT, with three peaks at 1.91, 2.76, and 3.67 Å, is significantly different from that for the original, colorless, oxidized solution of Eu-α-1 shown in Figure 5. The fit to the $k^3\chi(k)$ EXAFS with a three-coordination shell model with O nearest neighbors and distant P neighbors is quite good (dashed line in Figure 7). Fitting with S in place of P, to account for the possibility that the electrolyte, 0.2 M $[SO_4]^{2-}$, coordinates with Eu(III) produces equivalent fits and metrical parameters. Because P ($Z = 15$) and S ($Z = 16$) are adjacent elements, the use of EXAFS alone provides insufficient contrast to distinguish between P/S backscattering. The coordination of Eu(III) in the blue solution at −1.00 V is well-described by a first shell of 9.0 ± 1 O atoms at 2.42(2) Å, a second shell of 3.9 ± 0.9 P/(S) atoms at 3.16(3) Å, and a third shell of 1.8 ± 0.8 P/(S) atoms at 4.15(3) Å. All of the fitting parameters are provided in Table 2.

Despite the availability of such structural detail, the exact speciation of Eu(III) in terms of the identity, nature, and

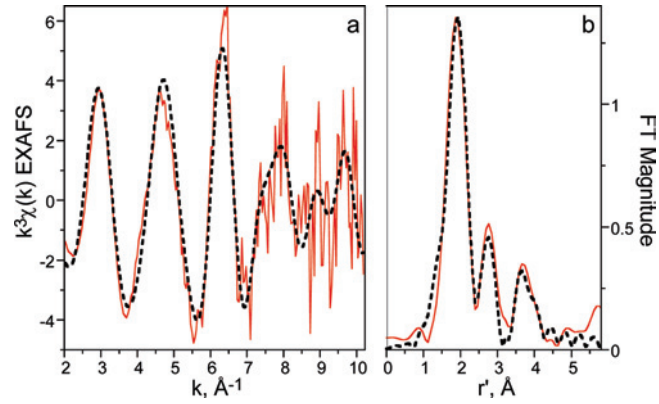

Figure 7. Eu L_3-edge $k^3\chi(k)$ EXAFS data (a) and corresponding Fourier transform data (b) for the blue solution of Eu-α-1 obtained by oxidation at −1.00 V of the fully reduced 5.0 mM analyte. The solid lines illustrate the experimental data, and the dashed lines show the fit.

Table 3. ^{31}P NMR Data for Original Eu-α-1 Solution (5.0 mM) before Reduction and for the Oxidized Eu-α-1 Solution Obtained after Reduction to the Heteropoly Blue Species with an Electrode Potential of −1.30 V[a]

solution	species	^{31}P NMR data (δ, ppm)
original Eu-α-1	$[(H_2O)_4Eu(\alpha\text{-}1\text{-}P_2W_{17}O_{61})]^{7-}$	6.42, −11.41
oxidized Eu-α-1	$[(H_2O)_4Eu(\alpha\text{-}1\text{-}P_2W_{17}O_{61})]^{7-}$	6.687, −11.34
	$[(H_2O)_nEu(PW_{11}O_{39})]^{4-}$	5.413[27]
	$[Eu(PW_{11}O_{39})_2]^{11-}$	0.416[27]
	$[Eu(\alpha\text{-}2\text{-}P_2W_{17}O_{61})_2]^{17-}$	3.747, −12.711[40]
	$[\alpha\text{-}1\text{-}P_2W_{17}O_{61}]^{10-}$	−8.54, −12.853[45]
	$\alpha\text{-}[P_2W_{18}O_{62}]^{6-}$	−12.467

[a] ^{31}P Spectra were referenced to 85% H_3PO_4.

number of different species is impossible to ascertain. The EXAFS data are consistent with a combination of P-containing species that are known decomposition products of α-1 and chelants of Eu, including $[P_2W_{18}O_{62}]^{6-}$, $[\alpha\text{-}2\text{-}P_2W_{17}O_{61}]^{10-}$, $[H_2P_2W_{12}O_{48}]^{12-}$,[45] as well as Eu phosphate/(sulfate) materials.[87,88] Additional spectroscopic evidence obtained by use of optical luminescence and ^{31}P NMR spectroscopy was applied to disentangle the identities of the individual species produced following the complete reduction and subsequent oxidation of Eu-α-1. This combination of techniques, wherein luminescence opens a window on the speciation of Eu only, and NMR on P speciation, provides information that complements and is otherwise not available from CV and Eu XANES.

Optical Luminescence. The bulk electrolysis experiment monitored by XANES was replicated and probed by luminescence spectroscopy to interrogate the Eu(III) speciation upon reduction and oxidation. The excitation spectrum of a fresh solution of Eu-α-1 in its oxidized (colorless) form prepared by dissolution of a spectroscopically pure solid salt, as determined by ^{31}P NMR (Table 3), in 0.2 M Li_2SO_4 (pH 3.0) is shown in Figure 8 (pink trace). The intense peak at 580.0 nm with a single-exponential lifetime of 215 ± 21 μs is in agreement with previous results for the tetrahydrated anion, $[(H_2O)_4Eu(\alpha\text{-}1\text{-}P_2W_{17}O_{61})]^{7-}$.[30] The spectrum shows two characteristic shoulders on the left and right flanks (579.8 and 580.5 nm, respectively) of the peak that exhibit biex-

(87) Kolitsch, U.; Holtstam, D. *Eur. J. Mineral.* **2004**, *16*, 117–126.
(88) Wickleder, M. S. *Chem. Rev.* **2002**, *102*, 2011–2087.

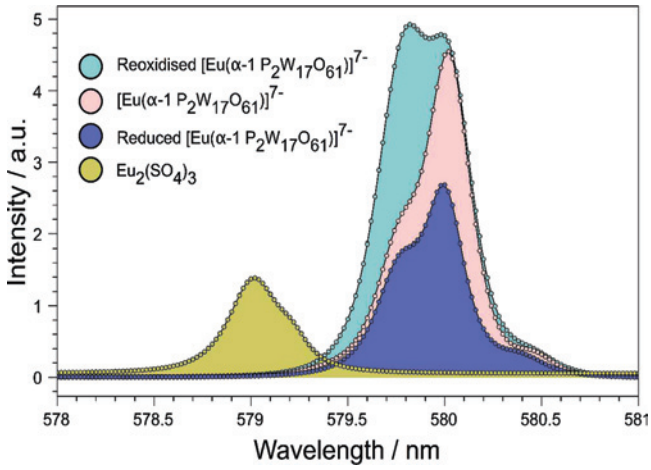

Figure 8. $^7F_0 \rightarrow {}^5D_0$ excitation spectrum ($\lambda_{em} = 614$ nm) of 47 μM solution of Eu-α-1 in 0.2 M Li_2SO_4 (pH 3.0) before reduction (pink trace), after reduction (blue trace), and after oxidation (teal trace). The corresponding excitation spectrum for $Eu_2(SO_4)_3$ is shown as the tan trace.

ponential lifetimes with components arising from $[(H_2O)_4Eu(\alpha\text{-}1\text{-}P_2W_{17}O_{61})]^{7-}$, and those attributed to the presence of isomeric species $[(H_2O)_nEu(\alpha\text{-}2\text{-}P_2W_{17}O_{61})]^{7-}$ and $[Eu(\alpha\text{-}2\text{-}P_2W_{17}O_{61})_2]^{17-}$, respectively.[30] The relatively small amount of isomerization (Figure S4, Supporting Information, for deconvolved spectrum) arises from the dilution-induced dissociation of Eu-α-1 at the extremely low concentration (47 μM) necessary to avoid quenching artifacts.[30]

The excitation spectrum of an aliquot of the blue, reduced solution removed from the electrochemical cell upon completion of exhaustive BE at −1.30 V in an identical manner to the in situ XAFS spectroelectrochemistry is shown in Figure 8 (blue trace). The dramatic decrease in signal intensity compared with that for the oxidized starting solution (pink trace) is attributed to the combination of two factors. First, the sample excitation and emission is attenuated by the deep-blue color of the solution, and second, the reduction of Eu(III) to Eu(II) lowers the Eu(III) concentration, which in turn lowers the luminescence intensities. Also the relative intensity of the shoulder at 579.7 nm on the left flank of the main peak at 580.0 nm increases to ca. two-thirds of the maximum peak value, consistent with the notion that reduction is correlated with decomposition. The lifetime, 320 ± 32 μs, of this shoulder is significantly longer than for the similar feature in the oxidized solution, 226 ± 22 μs, and suggests that a different species, notably $[(H_2O)_nEu(PW_{11}O_{39})]^{4-}$, forms upon reduction (Figure S5, Supporting Information).

The excitation spectrum for the solution following complete oxidation to its clear and colorless state is shown in Figure 8 (teal trace). The doublet spectrum with peaks of equal intensities at 579.8 and 580.0 nm and equal lifetimes, 258 ± 25 μs, indicates that the reduction−oxidation process induces the formation of bulk quantities of $[(H_2O)_nEu(PW_{11}O_{39})]^{4-}$. Because we thought it likely that the 0.2 M sulfate electrolyte would form an inner-sphere complex with any Eu(III) that disincorporates from the POMs, an excitation spectrum for a $Eu_2(SO_4)_3$ solution standard was obtained. As evident in Figure 8 (tan trace), the peak maximum for the excitation of $Eu_2(SO_4)_3$ occurs at 579.0 nm, which is well separated from the luminescence of the oxidized solution (teal trace). Therefore, we conclude that Eu(III)-$[SO_4]^{2-}$ complexation[89,90] does not pertain to the Eu-α-1 system as treated here (Figure S6, Supporting Information). Nevertheless, other isomeric Eu-POMs, besides $[(H_2O)_nEu(PW_{11}O_{39})]^{4-}$, are likely to contribute to the luminescence of the oxidized solution, Figure 8 (teal trace), as well. In view of uncertainties with multicomponent-lifetime analyses for such a polydisperse mixture, ^{31}P NMR was brought to bear upon the solution speciation.

NMR. A reduced and oxidized replication of the XANES experiment was monitored by ^{31}P NMR. The results of ^{31}P NMR measurements (Table 3 and Supporting Information (Figure S7)), demonstrate the presence of six POM species in the oxidized solution. These include the original Eu-α-1 complex and the free α-1 ligand as well as one product that results from isomerization and complexation, $[Eu(\alpha\text{-}2\text{-}P_2W_{17}O_{61})_2]^{17-}$, and three products that result from fragmentation and reconstitution, $[(H_2O)_nEu(PW_{11}O_{39})]^{4-}$, $[Eu(PW_{11}O_{39})_2]^{11-}$, and $\alpha\text{-}[P_2W_{18}O_{62}]^{6-}$. In view of the known chemical instabilities of the α-1 ligand,[45] the transformations to the Eu-α-2 and plenary Wells−Dawson anions are not unexpected. It is the formation of the two lacunary Keggin complexes of Eu(III) that are unusual and possibly driven by the combined Eu- and ligand-centered reductive electrochemistry of $[(H_2O)_4Eu(III)(\alpha\text{-}1\text{-}P_2W_{17}O_{61})]^{7-}$.

Conclusions

The Eu-α-1 POM combines an electroactive lanthanide ion, Eu(III), and an electroactive ligand, $[\alpha\text{-}1\text{-}P_2W_{17}O_{61}]^{10-}$, in a single, heterobinuclear molecular anion. The two redox-active centers involve valence orbitals of dissimilar character—localized 4f states of Eu and d-band states of W. The prospect of dual redox activity, although not always realized in Eu complexes with other electroactive ligands,[91,92] including POMs,[33,53] is demonstrated here for Eu-α-1, wherein the Eu(III)/Eu(II) couple occurs within the range of electrode potentials that drive the multielectron reduction of the P−W−O anion and the formation of a heteropoly blue species. Whereas the redox chemistry of the α-1 ligand is affected by its complexation with Eu(III), the redox chemistry of Eu is only slightly perturbed by its complexation with the ligand. Namely, for a dilute, 0.25 mM solution of Eu-α-1, the Eu(III)/Eu(II) couple is found at $E_{1/2} = -0.65$ V, which although deep within the domain of the W-centered redox processes (the first reduction occurs with $E_{1/2} = -0.33$ V) is essentially coincident with the electrode potential for the POM-free Eu(III) ion ($E_{1/2} = -0.63$ V) in the same supporting electrolyte of 0.2 M Li_2SO_4 at pH 3.0. The absence of a significant difference suggests that the energetics of the f-orbital interactions with the LUMO of essentially W d-orbital character are unfavorable and uncooperative, a possible result of insufficient interconnectivity. In this regard, the inner-sphere Eu coordination environment in the solid

(89) Tanaka, F.; Yamashita, S. *Inorg. Chem.* **1984**, *23*, 2044–2046.
(90) Vercouter, T.; Amekraz, B.; Moulin, C.; Giffaut, E.; Vitorge, P. *Inorg. Chem.* **2005**, *44*, 7570–7581.
(91) Kido, J.; Okamoto, Y. *Chem. Rev.* **2002**, *102*, 2357–2368.
(92) Richter, M. M.; Bard, A. J. *Anal. Chem.* **1996**, *68*, 2641–2650.

salt of Eu-α-1 and after its dissolution in the aqueous electrolyte were shown to be the same, consisting of four water molecules and the four O atoms from the tetradentate ligand with an average $Eu-O_8$ distance of 2.37−2.38 Å. The fact that the Eu cation is directly exposed to the solvent medium, although ideal for facile water exchange and electron transfer at an electrode surface, may account for its ligand-independent and labile behaviors, wherein the exhaustive, multielectron reduction of $[(H_2O)_4Eu(III)(\alpha\text{-}1\text{-}P_2W_{17}O_{61})]^{7-}$ to its metastable $[(H_2O)_nEu(II)(\alpha\text{-}1\text{-}P_2W_{17}O_{61})]^{n-}$ species leads to dynamic processes of Eu-disincorporation, cluster isomerization, fragmentation, and reconstitution to four other POMs, including $[Eu(\alpha\text{-}2\text{-}P_2W_{17}O_{61})_2]^{17-}$, $[(H_2O)_n\text{-}Eu(PW_{11}O_{39})]^{4-}$, $[Eu(PW_{11}O_{39})_2]^{11-}$, and $\alpha\text{-}[P_2W_{18}O_{62}]^{6-}$. Despite the apparent stability of the reduced species under conditions and on time scales typical of voltammetric measurements that show evidence of quasi-reversible redox chemistry, the significant instability of the fully reduced anion following controlled-potential bulk electrolysis leads to irreversible electroanalytical behaviors. A more-suitable medium, such as aprotic nonaqueous solvents, may improve the stability of the electrolyzed species. In this regard, efforts to understand the mechanism of the independent, reductive electrochemistry of Eu(III) and polyoxotungstates are underway.

Acknowledgment. We thank Dr. Nadia Leyarovska for generous assistance at the APS Sector 12 beam line. We are grateful to Professor Janet R. Morrow, State University of New York at Buffalo, for use of laser instrumentation (NSF MRI-0321058). This work is supported by the U.S. Department of Energy, Office of Basic Energy Science, Division of Chemical Sciences, Biosciences and Geosciences, under contract No. DE-AC02-06CH11357 (for the parts performed at Argonne National Laboratory); and by the NSF (Grant No. CHE 0414218) and NIH (S06 GM60654 (SCORE)) for the parts performed at Hunter College. Research Infrastructure at Hunter College is partially supported by NIH Research Centers in Minority Institutions Grant RR03037-08.

Supporting Information Available: Figures and tables containing details about cyclic voltammetry, optical luminescence, and NMR spectroscopy. This material is available free of charge via the Internet at http://pubs.acs.org.

IC800465E